Universal Journal of Fluid Mechanics **2 (2014), 55-68**
www.papersciences.com

MHD Non-linear Boundary Layer Flow and Heat Transfer of Nanofluids Past a Permeable Moving Flat Surface with Thermal Radiation and Viscous Dissipation

Winifred Nduku Mutuku
Mathematics Department, Kenyatta University, P. O. Box 43844
Nairobi, Kenya
mutukuwinnie@gmail.com

Abstract
By the current analysis, magnetohydrodynamic (MHD) boundary layer flow and heat transfer over a permeable moving surface due to a nanofluid with the effects of thermal radiation and viscous dissipation has been investigated. The model transport equations used in the analysis incorporates the effects of Brownian motion and thermophoresis. The governing non-linear boundary layer equations of the problem are formulated and transformed into coupled higher order non-linear ordinary differential equations using similarity transformation. The resultant equations are then solved numerically using fourth order Runge–Kutta method along with shooting technique. Graphical results elucidating the effects of various thermophysical parameters on the velocity, temperature, skin friction, Nusselt number and Sherwood number are presented and discussed quantitatively taking into account the industrial and engineering applications. It is noted that increasing magnetic field, radiation, viscous dissipation, thermophoresis and Brownian motion parameters leads to an increase the fluid temperature hence a reduction in the reduced Nusselt number. A comparison with previous studies available in the literature has been done and an excellent agreement established.

Keywords: Magnetohydrodynamic (MHD), Boundary Layer Flow, Heat Transfer, Nanofluids, Thermal Radiation, Viscous Dissipation.

1. Introduction

Boundary layer flow of an electrically conducting fluid over a moving surface in a uniform stream of fluid has been studied extensively due to its numerous industrial and engineering applications, such as: aerodynamic extrusion of plastic sheet, in metallurgy, cooling of an infinite metallic plate in a cooling bath, polymer extrusion, cooling or drying of papers and in textile and glass fiber production. It is argued that quality of final product in engineering and industrial processes largely depends upon the rate of cooling. The simultaneous effects of heat transfer and magnetohydrodynamic (MHD) are useful in order to achieve the final product of desire characteristics. Such considerations are very important especially in the metallurgical processes including the cooling of continuous strips and filaments drawn through a quiescent fluid and purification of molten metals from nonmetallic inclusions. Moreover, experimental and theoretical investigations on conventional electrically conducting fluids indicate that magnetic field markedly changes their transport and heat transfer characteristics. Since the pioneering work of Hartmann and Lazarus [1] on the hydromagnetic flow of a viscous electrically conducting liquid, several authors [2-4] have investigated the problem under different flow conditions. Meanwhile, the heat transfer performance of these conventional fluids (such as water, minerals oil, ethylene glycol, etc.,) is often limited due to their low thermal conductivities. With the rising demands of modern technology for process intensification, an innovative technique which involves dispersing small amounts of nanometer-sized (10–50 nm) particles and fibers in conventional base fluids was introduced by Choi [5] in order to enhance their heat transfer performance. Nanofluid is envisioned to describe a fluid in which nanometer sized particles are suspended in convectional heat transfer base fluids. Several theoretical and experimental results have shown that nanofluids possess enhanced thermophysical properties such as thermal conductivity, thermal diffusivity, viscosity and convective heat transfer coefficients as compared to those of conventional base fluids [6-8]. The

remarkably improved convective heat transfer coefficient makes the nanofluid a superior heat transfer medium for cooling applications such as in advanced nuclear systems, and cylindrical heat pipes. Suction of a fluid through the bounding surface, as, for example, in mass transfer cooling, can significantly change the flow field and, as a consequence, affect the heat transfer rate at the surface. In general, suction tends to increase the skin friction and heat transfer coefficients [9].

Radiation effects is very significant especially at high operating temperatures encountered in the field of space technology. The knowledge of radiative heat transfer has becomes very important, particularly in designing pertinent equipment for use in engineering processes involving high temperatures. As a result, recent studies have incorporated effects of thermal radiation in their studies. Poornima and Reddy [10] studied steady free convective boundary layer flow of a radiating nanofluid along a non-linear stretching sheet in the presence of transverse magnetic field. Kandasamy et al. [11] investigated MHD boundary layer flow of a nanofluid in the presence of thermal stratification due to solar radiation taking into consideration the effects of Brownian motion and thermophoresis. More recently, Motsumi and Makinde [12] numerically investigated the effects of thermal radiation and viscous dissipation on boundary layer flow of nanofluids over a permeable moving flat plate. The current study aims to extend their recent work by examining the effects of thermal radiation and viscous dissipation on boundary layer and heat transfer of nanofluids over a permeable moving surface subjected to a magnetic field strength. In the following sections, the model is formulated, analysed and numerically solved. Pertinent results are presented graphically and discussed.

2. Mathematical Formulation

Consider the steady, laminar, incompressible, two-dimensional boundary layer flow of an electrically conducting nanofluid past a flat surface moving at a constant velocity U_w. We choose the coordinate system such that x-axis is along the horizontal plate and y-axis is orthogonal to the plate. The physical flow model and coordinate system is shown in Fig. 1. A transverse magnetic field of strength B_0 is applied parallel to the y- axis. There is no applied voltage and the magnetic Reynolds number is small, hence the induced magnetic field and Hall effects are negligible. The variable plate surface permeability function is defined by $V_w = -f_w\left(a\upsilon_f\right)^{1/2}$ where f_w is the suction/injection parameter, with $f_w > 0$ representing the transpiration (suction) rate at the plate surface, $f_w < 0$ corresponds to injection and $f_w = 0$ for an impermeable surface.

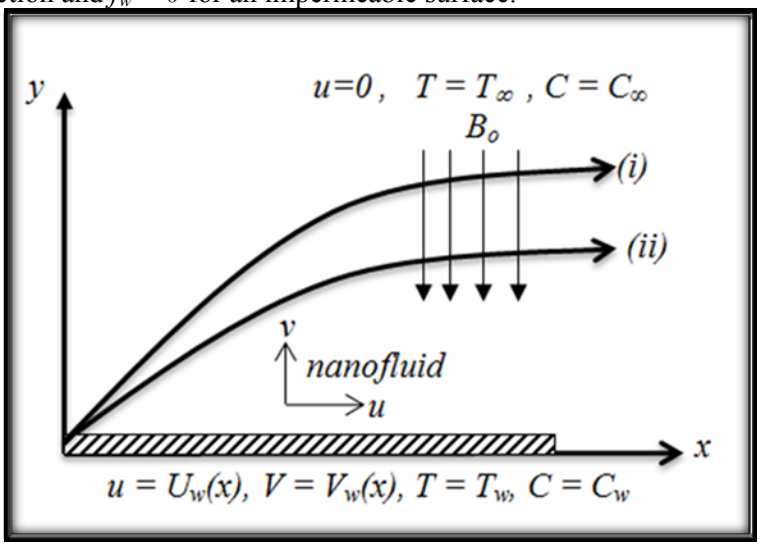

Fig. 1 Schematic Diagram of the Flow

Considering the nanofluid as a continuous media with thermal equilibrium and no slip occurring between the base fluid and the solid nanoparticles, the basic steady governing equations of continuity, momentum, thermal energy and nanoparticle concentration are given as:

$$\frac{\partial u}{\partial x}+\frac{\partial v}{\partial y}=0, \tag{2.1}$$

$$u\frac{\partial u}{\partial x}+v\frac{\partial u}{\partial y}=-\frac{1}{\rho_f}\frac{\partial p}{\partial x}+\upsilon\frac{\partial^2 u}{\partial y^2}-\frac{\sigma {B_o}^2 u}{\rho_f}, \tag{2.2}$$

$$\begin{aligned} u\frac{\partial T}{\partial x}+v\frac{\partial T}{\partial y}=\alpha\frac{\partial^2 T}{\partial y^2}+\frac{\mu}{\left(\rho c_p\right)_f}\left(\frac{\partial u}{\partial y}\right)^2+\frac{\sigma {B_o}^2 u^2}{\left(\rho c_p\right)_f} \\ -\frac{1}{\left(\rho c_p\right)_f}\frac{\partial q_r}{\partial y}+\tau\left\{D_B\frac{\partial C}{\partial y}\frac{\partial T}{\partial y}+\frac{D_T}{T_\infty}\left(\frac{\partial T}{\partial y}\right)^2\right\}, \end{aligned} \tag{2.3}$$

$$u\frac{\partial C}{\partial x}+v\frac{\partial C}{\partial y}=D_B\frac{\partial^2 C}{\partial y^2}+\frac{D_T}{T_\infty}\frac{\partial^2 T}{\partial y^2}, \tag{2.4}$$

with the boundary conditions,

$$\begin{aligned} &u=U_w(\mathrm{x})=ax, \quad \mathrm{v}=\mathrm{V}_w(\mathrm{x}), \quad T=T_w, \quad C=C_w \quad \text{at } \mathrm{y}=0 \\ &u\to 0, \qquad \mathrm{v}\to 0, \qquad T\to T_\infty, \quad C\to C_\infty \quad \text{as } \mathrm{y}\to\infty \end{aligned} \tag{2.5}$$

where u and v are the velocity components along the x- and y-directions respectively, t is time, T_w and C_w are temperature and nanoparticle volume fraction at the plate surface respectively, T_∞ and C_∞ are the free stream temperature and nanoparticle volume fraction respectively, ρ is the density, $\alpha = k/(\rho C_p)_f$ is the thermal diffusivity, k is the thermal conductivity, $\upsilon = \mu/\rho_f$ is the kinematic viscosity coefficient, μ is the dynamic viscosity, c_p is the specific heat at constant pressure, σ is the electrical conductivity, $\tau = (\rho C)_p/(\rho C)_f$ is the ratio of the effective heat capacitance of the nanoparticle to that of the base fluid, D_B is the Brownian motion coefficient, D_T is the thermophoretic coefficient, q_r is the radiative heat flux, C is the nanoparticle volume fraction.

Using the Rosseland approximation for the thermal radiation, the radiative heat flux is simplified as:

$$q_r=-\frac{4\sigma^*}{3k^*}\frac{\partial T^4}{\partial y}, \tag{2.6}$$

where σ^* is the Stephan–Boltzmann constant and k^* is the mean absorption coefficient.

The temperature differences within the flow are assumed to be sufficiently small such that T^4 may be expressed as a linear function of temperature T using a truncated Taylor series about the free stream temperature T_∞ as follows:

$$T^4 \cong 4{T_\infty}^3 T-3{T_\infty}^4 \tag{2.7}$$

Thus, substituting Equation (2.7) into Equation (2.6), we get:

$$q_r = -\frac{16T_\infty^{\,3}\sigma^*}{3k^*}\frac{\partial T}{\partial y}, \tag{2.8}$$

Using the boundary-layer approximations, and incorporating equation (2.8), the governing equations become:

$$\frac{\partial u}{\partial x}+\frac{\partial v}{\partial y}=0, \tag{2.9}$$

$$u\frac{\partial u}{\partial x}+v\frac{\partial u}{\partial y}=\upsilon\frac{\partial^2 u}{\partial y^2}-\frac{\sigma B_o^{\,2}u}{\rho_f}, \tag{2.10}$$

$$\begin{aligned} u\frac{\partial T}{\partial x}+v\frac{\partial T}{\partial y} &= \alpha\frac{\partial^2 T}{\partial y^2}+\frac{\mu}{\left(\rho c_p\right)_f}\left(\frac{\partial u}{\partial y}\right)^2+\frac{\sigma B_o^{\,2}u^2}{\left(\rho c_p\right)_f} \\ &+\frac{16\sigma^* T_\infty^{\,3}}{3k^*\left(\rho c_p\right)_f}\frac{\partial^2 T}{\partial y^2}+\tau\left\{D_B\frac{\partial C}{\partial y}\frac{\partial T}{\partial y}+\frac{D_T}{T_\infty}\left(\frac{\partial T}{\partial y}\right)^2\right\}, \end{aligned} \tag{2.11}$$

$$u\frac{\partial C}{\partial x}+v\frac{\partial C}{\partial y}=D_B\frac{\partial^2 C}{\partial y^2}+\frac{D_T}{T_\infty}\frac{\partial^2 T}{\partial y^2}, \tag{2.12}$$

Using the stream function $\psi=\psi(\mathrm{x},\mathrm{y})$, the velocity components *u* and *v* are defines as;

$$u=\frac{\partial\psi}{\partial y}\ \text{and}\ v=-\frac{\partial\psi}{\partial x} \tag{2.13}$$

By means of the following similarity transformations,

$$\begin{aligned} &\eta=\left(a/\upsilon_f\right)^{1/2}y, \quad \psi=\left(a\upsilon_f\right)^{1/2}xf(\eta), \\ &\theta(\eta)=\frac{T-T_\infty}{T_w-T_\infty},\ \phi(\eta)=\frac{C-C_\infty}{C_w-C_\infty}, \end{aligned} \tag{2.14}$$

the governing equations (2.9) – (2.12) together with the boundary conditions in equation (2.5) are transformed to ordinary differential equation as follows:

$$f'''+ff''-f'^2-Mf'=0 \tag{2.15}$$

$$\frac{1}{\mathrm{Pr}}\left(1+\frac{4}{3}R\right)\theta''+f\theta'+Ec\left(f''^2+Mf'^2\right)+Nb\theta'\phi'+Nt\theta'^2=0 \tag{2.16}$$

$$\phi''+Lef\phi'+\frac{Nt}{Nb}\theta''=0 \tag{2.17}$$

The corresponding boundary conditions are;

$$\begin{aligned} &f(0)=f_w,\quad f'(0)=1,\quad \theta(0)=1,\qquad \phi(0)=1, \\ &f(\infty)=0,\qquad \theta(\infty)=0,\qquad \phi(\infty)=0, \end{aligned} \tag{2.18}$$

where prime denotes differentiation with respect to η. f', θ, ϕ are the dimensionless velocity, temperature and nanoparticle concentration respectively. *Pr*, *R*, *Ec*, *M*, *Nb*, *Nt* and *Le* denote Prandtl number, radiation parameter, magnetic parameter, Eckert number, Brownian motion parameter, thermophoresis parameter and Lewis number respectively and are defined as:

$$M=\frac{\sigma B_0^2}{\rho_f a},\quad Nb=\frac{(\rho c)_p D_B (C_w-C_\infty)}{\upsilon(\rho c)_p},\quad Nt=\frac{(\rho c)_p D_T (T_w-T_\infty)}{\upsilon(\rho c)_p T_\infty},$$
$$Ec=\frac{U_w^2}{C_p(T_w-T_\infty)},\quad \Pr=\frac{\upsilon}{\alpha},\quad R=\frac{4\sigma^* T_\infty^3}{k^* k},\quad Le=\frac{\upsilon}{D_m}, \tag{2.19}$$

For the type of boundary layer flow under consideration, the skin-friction coefficient, Nusselt number and Sherwood number are important physical parameters. The skin friction coefficient C_f, the local Nusselt number Nu_x and the local Sherwood number Sh_x are defined respectively as:

$$C_f=\frac{\tau_w}{\rho U_w^2},\quad Nu_x=\frac{xq_w}{k(T_w-T_{o,\infty})},\quad Sh_x=\frac{xq_m}{D_B(C_w-C_{o,\infty})}, \tag{2.20}$$

where the wall shear stress τ_w, the wall heat flux q_w and the wall mass flux q_m are given by;

$$\tau_w=\mu\left.\frac{\partial u}{\partial y}\right|_{y=0},\ q_w=-k\left.\frac{\partial T}{\partial y}\right|_{y=0},\quad q_m=-D_B\left.\frac{\partial C}{\partial y}\right|_{y=0}. \tag{2.21}$$

By using equation (2.21) into (2.20) we get,

$$\mathrm{Re}_x^{1/2} C_f = f''(0),\quad \mathrm{Nur}=\mathrm{Re}_x^{-1/2} Nu_x=-\theta'(0),\quad \mathrm{Shr}=\mathrm{Re}_x^{-1/2} Sh_x=-\phi'(0), \tag{2.22}$$

which are the local skin friction C_f, reduced Nusselt number *Nur* and reduced Sherwood number *Shr* respectively and $Re_x = U_\infty x/\upsilon$ is the local Reynolds number.

3. Numerical solution

An efficient fourth order Runge–Kutta integration scheme with a systematic guessing of $f''(0),\ \theta'(0),\ \phi'(0)$ by a modified version of the Newton-Raphson shooting technique until the boundary conditions at infinity $f''(\infty),\ \theta'(\infty),\ \phi'(\infty)$ decay exponentially to zero, has been employed to numerically solve the set of coupled non-linear ordinary differential equations equations (15) – (17) with boundary conditions (18). The computations were done by a program which uses a symbolic and computational computer language Maple. This method involves, transforming the coupled ordinary differential equations (15) – (17) which are third order in f and second order in θ and ϕ to a system of seven simultaneous equations with seven unknowns. To numerically solve the resultant system of equations using Runge-Kutta integration scheme, seven initial conditions are required, but two initial conditions in f, one initial condition in each of θ and ϕ are known. However, the values of $f''(\infty),\ \theta'(\infty),\ \phi'(\infty)$ can be utilised to generate unknown initial conditions at $\eta = 0$ by using shooting technique. The step size $\Delta\eta = 0.001$ is used while obtaining the numerical solution with η_∞, and accuracy to the fifth decimal place is sufficient for convergence. To estimate the value of η_∞, we start with some initial guess value and solve the boundary value problem consisting of equations (15) – (17) to obtain f'', θ, ϕ' at $\eta = 0$. The value of was found in each iteration loop by using $\eta_\infty = \eta_\infty + \Delta\eta$ values for consecutive steps until two successive values of f'', θ, ϕ' at $\eta = 0$ do not change error less than 10^{-7}.Once all suitable initial conditions are obtained, the system of simultaneous equations is solved using fourth order Runge–Kutta integration scheme.

Now we can define new variables by the equations:

$$f_1=f,\ f_2=f',\ f_3=f'',\ f_4=\theta,\ f_5=\theta',\ f_6=\phi,\ f_7=\phi' \tag{3.1}$$

The set of higher order non-linear boundary value problem with their respective boundary conditions are reduced to seven equivalent first order differential equations with appropriate initial conditions, respectively, as given below:

$$
\begin{aligned}
f_1 &= f_2, \\
f_2' &= f_3, \\
f_3' &= -f_1 f_3 + f_2^2 + M f_2, \\
f_4' &= f_5, \\
f_5' &= \Pr \frac{\left[-f_1 f_5 - Ec\left\{ f_3^2 + f_2^2 \right\} - Nb f_5 f_2 - Nt f_5^2 \right]}{\left(1 + \frac{4}{3} R \right)}, \\
f_6' &= f_7, \\
f_7' &= -Le f_1 f_7 + \frac{Nt}{Nb} \Pr \frac{\left[-f_1 f_5 - Ec\left\{ f_3^2 + f_2^2 \right\} - Nb f_5 f_2 - Nt f_5^2 \right]}{\left(1 + \frac{4}{3} R \right)},
\end{aligned} \tag{3.2}
$$

subject to the initial conditions:

$$
\begin{aligned}
&f_1(0) = f_w, f_2(0) = 0, \; f_3(0) = s_1, f_4(0) = 1, \\
&f_5(0) = s_2, f_6(0) = 1, f_7 = s_3,
\end{aligned} \tag{3.3}
$$

By applying the shooting method, the unspecified initial conditions S_1, S_2 and S_3 in (3.3) are assumed and (3.2) integrated numerically as an initial valued problem to a given terminal point. The accuracy of the assumed missing initial conditions was checked by comparing the calculated value of the dependent variable at the terminal point with its given value there. If differences exist, improved values of the missing initial conditions are obtained and the process repeated. The results obtained are presented through tables and graphs, and the main features of the problems are discussed and analyzed.

4. Results and Discussion

In order to get a physical insight into the problem, a parametric study is conducted to illustrate the effects of different governing parameters viz., the magnetic parameter M, the radiation parameter R, the Prandtl number Pr, the Lewis number Le, suction/injection parameter f_w, the thermophoretic parameter Nt and the Brownian motion parameter Nb upon the nature of flow and transport and the numerical results are depicted graphically and in tabular form in figs.2-10 and table 2 respectively. Here the value of Pr is chosen as 0.71, which corresponds to air. To validate our results comparison has been done with Poornima and Reddy [10] and Khan and pop [13]. We notice that the comparison shows good agreement , therefore, we are confident that the present results are very accurate.

Table 1: Comparison of reduced Nusslet number and Reduced Sherwood number for R=0, Ec=0, f_w=0.

Nb	**Nt**	**Pr**	**Le**	**M**	**Khan and pop (2012)**		**Poornima and Reddy (2013)**		**Present**	
					$-\theta'(0)$	$-\phi'(0)$	$-\theta'(0)$	$-\phi'(0)$	$-\theta'(0)$	-□ (0)
0.1	0.1	10	10	1	0.9524	2.1294	0.952376	0.952376	0.9524	2.1294
0.2	0.2	10	10	1	0.3654	2.5152	0.365357	0.365357	0.3654	2.5152
0.3	0.3	10	10	1	0.1355	2.6088	0.135514	0.135514	0.1355	2.6088
0.4	0.4	10	10	1	0.0495	2.6038	0.049465	0.049465	0.0495	2.6038
0.5	0.5	10	10	1	0.0179	2.5731	0.017922	0.017922	0.0179	2.5731

4.1. Effects of parameters variation on the velocity profiles

Figs. 1-2 show the velocity profile f' for different values of the magnetic field parameter M and suction/injection parameter f_w respectively. Fig. 1 reveals that increasing the magnetic field retards the fluid velocity. This result qualitatively agrees with the expectations, since magnetic field exerts a retarding force on the natural convection flow. The presence of a transverse magnetic field to an electrically conducting fluid give rise to a resistive-type force called the Lorentz force. This force has the tendency to slow down the motion of the fluid and to increase its temperature profiles. As the values of magnetic parameter M increase, the retarding force increases and consequently the motion of the fluid decreases and the momentum boundary layer increases. A similar behaviour is noted with increasing values of suction parameter $f_w < 0$. The explanation for such behavior is that the fluid is brought closer to the surface and as such the presence of wall suction decreases both the fluid velocity and velocity boundary layer thickness. However, the exact opposite behavior is produced by imposition of wall fluid blowing or injection.

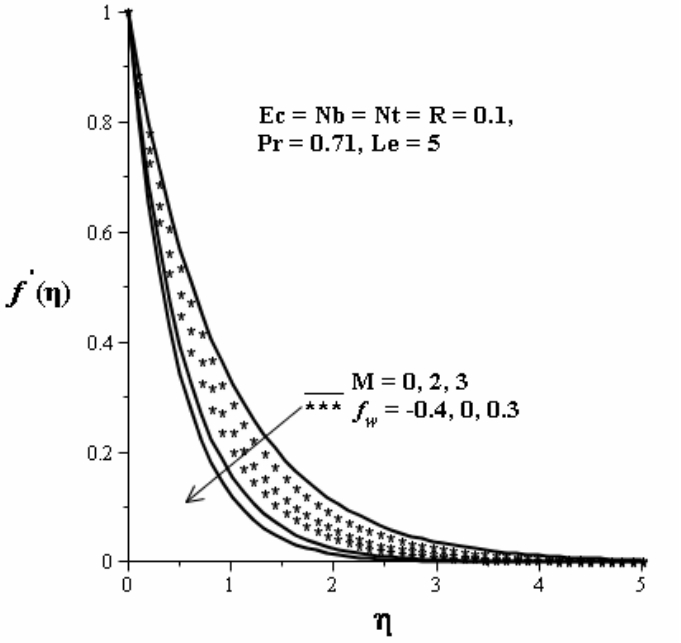

Fig. 2 Velocity profile for different values for M and f_w

4.2. Effects of parameters variation on the temperature profiles

Figs. 3-6 depict the influences of pertinent parameters of the fluid temperature. It is revealed that the temperature is maximum at the plate surface but decreases to zero far away from the plate surface satisfying the free stream conditions. Fig. 3 depicts the effects of Prandtl number and sunction/injection parameter on the temperature profile. It is worth noting that the liquid metals are characterized by small values of Pr (< 1),which are highly conducive and have low viscosity, while large values of Pr (≥1) represent high viscosity oils. Specifically, Prandtl number Pr=0.72, 1.0 and 7.0 correspond to air, electrolyte solution such as salt water and water, respectively [14].

It is observed that an increase in Prandtl number Pr and suction/injection parameter f_w, results in a decrease in both the temperature distribution and the thermal boundary layer thickness. An increase in Pr leads to a shift in the profiles towards the boundary causing a diminution in the thickness of thermal boundary layer. Physically this is attributed to the fact that higher Prandtl number fluid has a relatively lower thermal conductivity which reduces conduction and thereby increases the variations of thermal characteristics. An increase in the Prandtl number means slow rate of thermal diffusion, thus, smaller values of Pr are equivalent to larger values of thermal conductivities and therefore heat is able to

diffuse away from the moving surface. This results in the reduction of the thermal boundary layer thickness and increase in the heat transfer at the moving surface. The effect of Prandtl number on a nanofluid is similar to what is typically observed in common fluids qualitatively but they are different quantitatively. Thus, it can be concluded that these properties are inherited by nanofluids. Increasing the suction parameter means that more nanofluid is sucked through the permeable surface to the surrounding, hence, a reduction in thermal and nanoparticle volume boundary layer thickness is expected, i.e. the presence of wall suction thins out the thermal and nanoparticle volume fraction boundary layers. However, the exact opposite behavior is produced by wall fluid blowing or injection. On the contrary, both the temperature and the thermal boundary layer thickness increase with increasing values of magnetic parameter *M*, radiation parameter *R*, thermophoresis parameter *Nt*, Brownian motion parameter *Nb* and Eckert number *Ec*. This can be attributed to internal heat generation within the nanofluid due resistance of fluid flow as a result of the Lorentz force, the presence of the nanoparticle and additional heating as a result of the viscous dissipation. This increase in temperature at the plate surface implied that, the local Nusselt number $-\theta'(0)$, which represents the heat transfer rate at the surface subsequently decreases. This is due to the fact that the thermophoresis Parameter *Nt* is directly proportional to the heat transfer coefficient associated with the nanofluid. It is interesting to note that Brownian motion of nanoparticles at the molecular and nanoscale levels is a key nanoscale mechanism governing their thermal behavior. In nanofluid systems, due to the size of the nanoparticles Brownian motion takes place which can affect the heat transfer properties. As the particle size scale approaches to the nanometer scale, the particle Brownian motion and its effect on the surrounding liquids play an important role in heat transfer. The radiation parameter *R* is the measure of the relative importance of the thermal radiation transfer to the conduction heat transfer. Thus larger values of *R* show a dominance of the thermal radiation over conduction. Consequently larger values of *R* are indicative of larger amount of radiative heat energy being poured into the system, causing a rise in the temperature of the flow field.

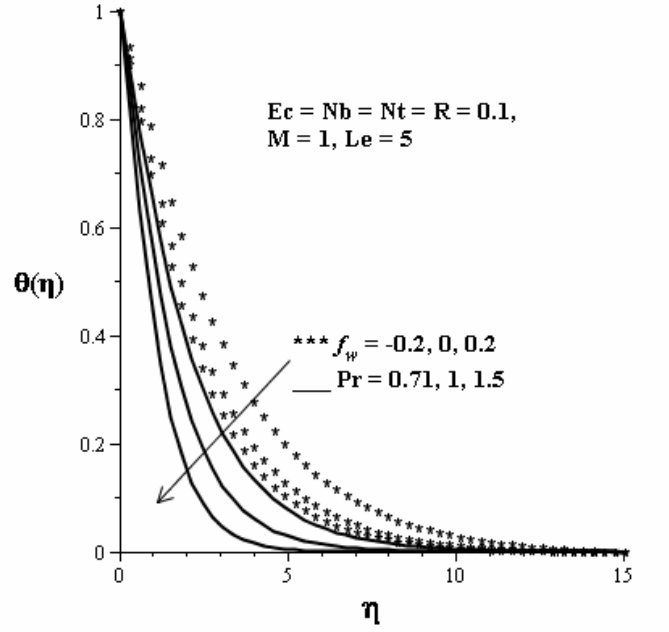

Fig. 3 Temperature profile for different values for Pr and f_w

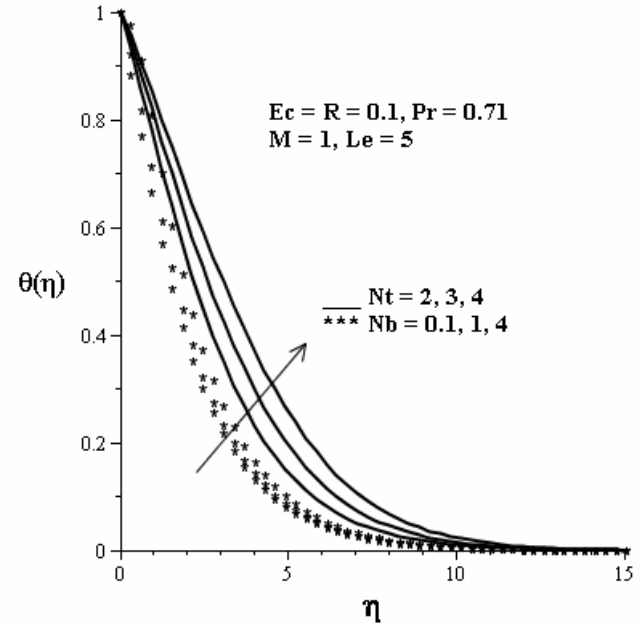

Fig. 4 Temperature profile for different values for Nt and Nb

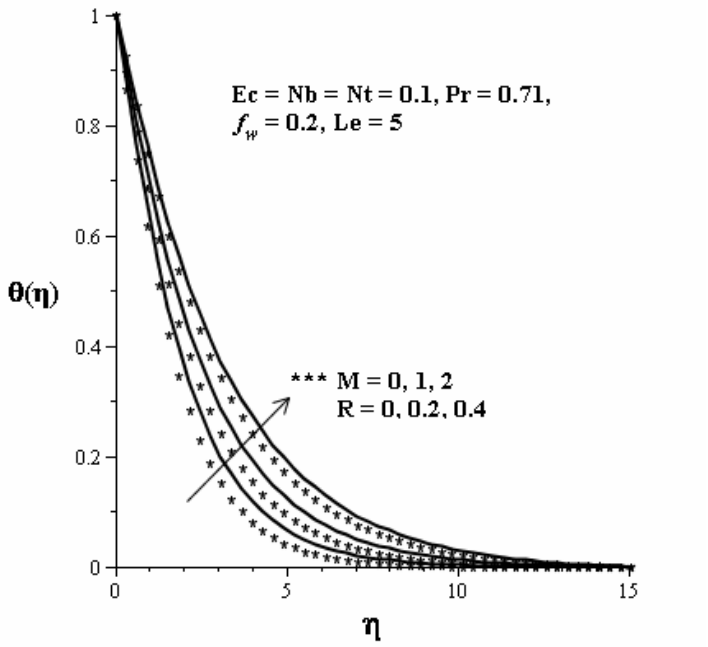

Fig. 5 Temperature profile for different values for M and R

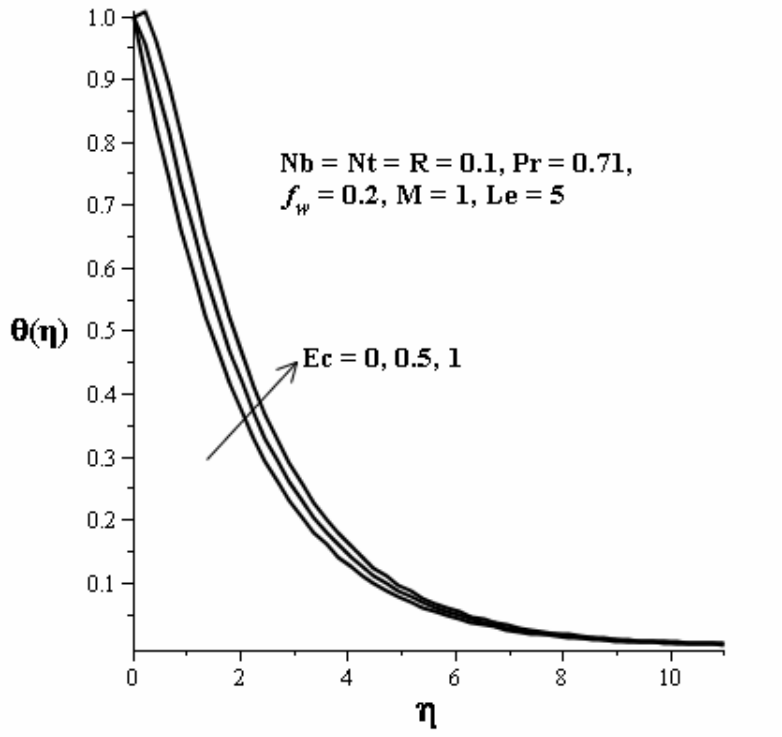

Fig. 6 Temperature profile for different values for Ec

4.3. Effects of parameter variation on nanoparticle concentration profiles

The effects of different values of governing parameters on the nanoparticle concentration profile are depicted in figs. 8-10. It is noted from fig. 8, the nanoparticle concentration increases with increase in magnetic parameter *M*, thermophoresis parameter *Nt*, and Prandtl *Pr*. This implies that the magnitude of concentration gradient on the surface of a sheet decreases as well. Thus, the local Sherwood number $-\phi'(0)$, which represents the mass transfer rate at the surface decreases with increase in *M*, *Nt* and *Pr*. It is well known that, thermophoresis parameter *Nt* increases the mass transfer of a nanofluids, consequently, mass transfer rate at a surface decreases. It is worth noting that positive *Nt* indicates a cold surface, while negative to a hot surface. For hot surfaces, thermophoresis tends to blow the nanoparticle volume fraction boundary layer away from the surface since a hot surface repels the sub-micron sized particles from it, thereby forming a relatively particle-free layer near the surface, while for cold surfaces the reverse will occur. As a result thermophoresis effect is among the important parameters constituting natural convection of nanofluids. On the other hand, increasing the Lewis number *Le*, the Brownian motion parameter *Nb* and the radiation parameter *R*, tends to cause a decrease in both the concentration profile and the concentration boundary layer thickness as seen in fig. 9.

The massive decrease in the nanoparticles concentration at the surface with increasing values of *Nb*, is not surprising since the increasing values of *Nb* give rise to the effective movement of nanoparticles from the sheet to the fluid. Fig. 9, also reveals that a decrease in the mass fraction field is observed with an increase in suction ($f_w>0$), while injection ($f_w<0$) causes an increase in the nanoparticle volume fraction.This decrease in the concentration profile can be attributed to the fact that increasing *Le*, *Nb*, and *R* increases the mass transfer rate, consequently increasing the concentration gradient at surface. Moreover, the concentration at the surface decreases as the values of *Le*, *Nb*, and *R* increase. Fig. 10 illustrates the variation of Eckert number *Ec* on the concentration graph. At the boundary layer region, an increase is noted with increasing values of *Ec*, while the reverse is observed as one moves towards the free stream.

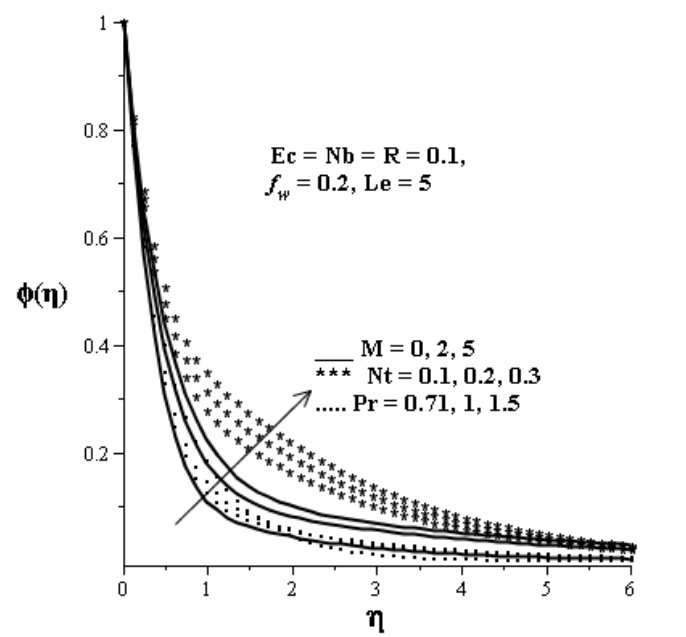

Fig. 7 Nanoparticle concentration for different values for M, Nt and Pr

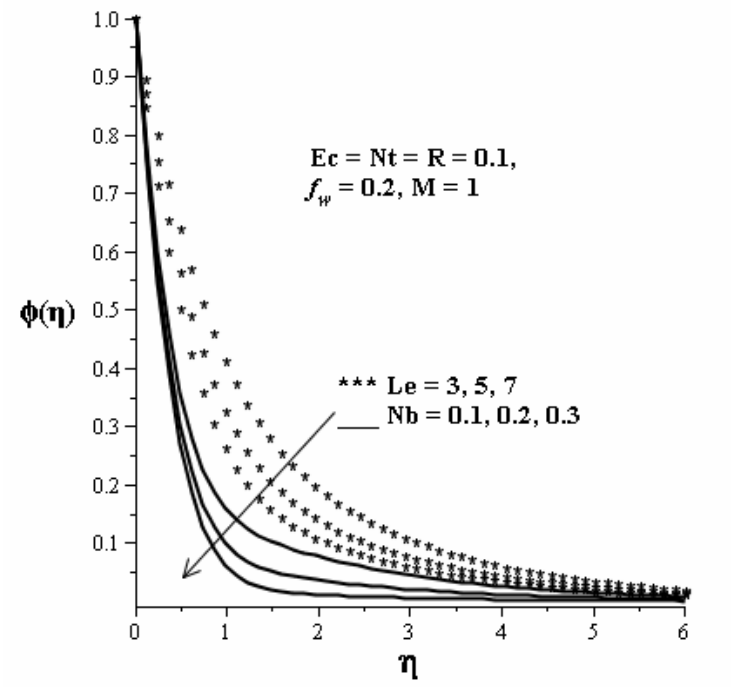

Fig. 8 Nanoparticle concentration for different values for Le and Nb

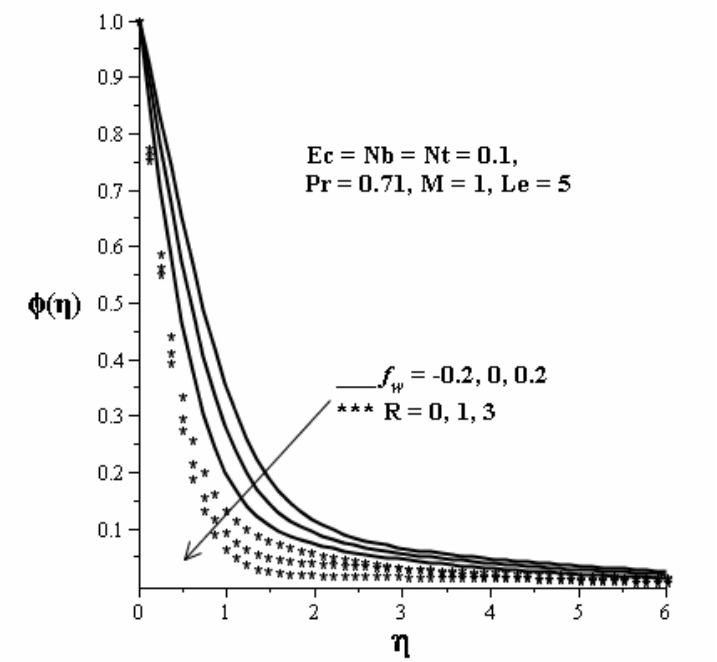

Fig. 9 Nanoparticle concentration for different values for f_w and R

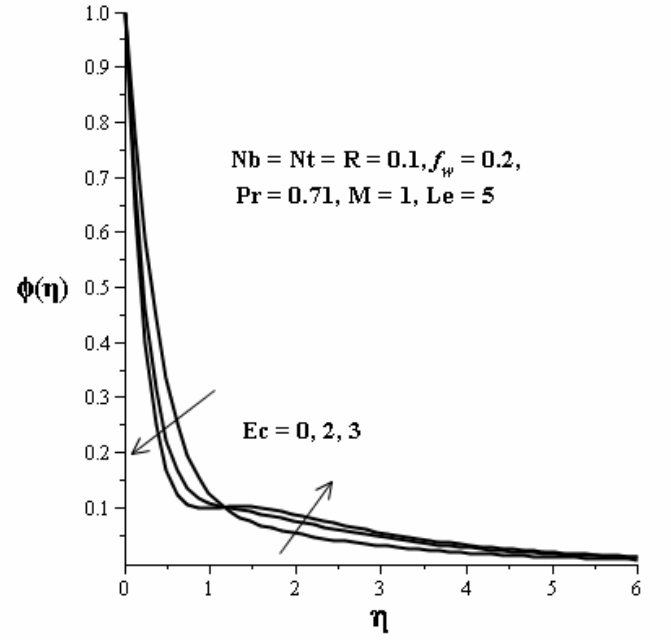

Fig. 10 Nanoparticle concentration for different values for Ec

4.4. Effects of parameters variation on the skin friction C_f, Nusselt number *Nur* and Sherwood number *Shr*.

Table 2 shows the effects of various governing parameters on the skin friction coefficient, reduced Nusselt number and the reduced Sherwood number. Nusselt number and Sherwood number are synonymous to the heat transfer rate and mass transfer rate at the surface of the plate respectively. It is

observed that, increasing M, increases C_f but leads to a decrease in both *Nur* and *Shr*. Increasing f_w, increases all the important physical parameters, C_f, *Nur* and *Shr*. No effect is noted in C_f with increasing values of *R*, *Pr*, *Nb*, *Nt*, *Le* and *Ec*. However, increasing *Pr*, leads to an increase in *Nur* but a decrease in *Shr*. This result qualitatively agrees with the expectations, since a higher Prandtl number fluid has a relatively lower thermal conductivity, which reduces conduction and thereby increases the heat transfer rate at the surface. An increase in *Nb* decreases both *Nur* and *Shr*. A decrease in *Nur* and an increase in *Shr* is observed with increasing values of *Nt, Le* and *Ec*.

Table 2: Computation showing the values skin friction coefficient $-f''(0)$, reduced Nusslet number $-\theta'(0)$ and reduced Sherwood number $-\phi'(0)$ for varying governing parameters

M	**R**	**Pr**	**Nb**	**Nt**	**Ec**	**Le**	**f_w**	$-f''(0)$	$-\theta'(0)$	$-\phi'(0)$
0	0.1	0.71	0.1	0.1	0.1	5	0.2	1.1054	0.4391	2.0681
1								1.5177	0.3610	2.0248
2								1.8349	0.3109	1.9948
3								2.1025	0.2736	1.9718
4								2.3383	0.2439	1.9531
1	**0**							1.5177	0.3888	2.0060
	1							1.5177	0.2535	2.1062
	2							1.5177	0.2191	2.1372
	5							1.5177	0.1903	2.1664
	0.1	**0.71**						1.5177	0.3610	2.0248
		1						1.5177	0.4443	1.9699
		1.5						1.5177	0.5707	1.8918
		0.71	**0.1**					1.5177	0.3610	2.0248
			0.3					1.5177	0.3386	1.7341
			0.5					1.5177	0.3179	1.5009
			0.1	**0.1**				1.5177	0.3610	2.0248
				0.3				1.5177	0.2819	2.0115
				0.5				1.5177	0.2495	2.1104
				0.1	**0**			1.5177	0.3784	1.2486
					0.3			1.5177	0.1963	2.0073
					0.6			1.5177	0.0128	2.7717
					0.1	**2**		1.5177	0.3648	0.8952
						5		1.5177	0.3610	2.0248
						8		1.5177	0.3599	2.9571
						5	**-0.2**	1.3177	0.2216	0.8451
							0	1.4142	0.2876	1.3869
							0.2	1.5177	0.3610	2.0248

5. Conclusions

This paper presents a numerical analysis of combined effects of magnetic field intensity, thermal radiation, viscous dissipation and suction on the heat transfer and thermal boundary layer flow of a

nanofluid over a moving flat surface. The model used for the nanofluid incorporates the effects of Brownian motion and thermophoresis. The governing nonlinear partial differential equations were transformed into ordinary differential equations using a similarity approach and solved numerically using the Runge–Kutta–Fehlberg method coupled with the shooting technique.The Numerical results for dimensionless parameters as well as the skin-friction coefficient and Nusselt number, are presented graphically and analysed quantitatively. Based on the graphical representations, the following important conclusions are summarized:

- The fluid field is retarded by increasing the magnetic field strength and the suction parameter.
- There is an increase in the temperature profile with increase in magnetic field strength, thermosphoresis, Brownian motion, radiation parameters and Eckert number but the contrary is observed with increase in suction and Prandtl number.
- The nanoparticle concentration increases with increase in magnetic field strength, thermosphoresis parameter and Prandtl number, but decreases with increase in Brownian motion, suction, radiation parameters, Lewis number, and Eckert number.
- There is an increase in skin friction coefficient with increase in magnetic field strength and suction.
- The rate of heat transfer is increased with increase in Prandtl number and suction parameter, but decreases with increase in magnetic field strength, thermosphoresis, Brownian motion, radiation parameters, Eckert number and Lewis number.
- An increase in Sherwood number is observed with increasing values of radiation, thermosphoresis, suction parameters, Lewis number, Eckert number, while a decrease is noted with increasing values of magnetic field strength, Brownian motion parameter and Prandtl number.

References

1. *Hartmann J., Lazarus F.,*'Kongelige danske videnskabernes selskab', *Matematisk Fsiske Meddelelser,* ***15*** *(1937), 6–7.*
2. *Makinde O.D.,*'On MHD heat and mass transfer over a moving vertical plate with a convective surface boundary condition', *Can. J. Chem. Eng.,* ***88*** *(2010), 983–990.*
3. *Rajput G. R., Prasad J. S. V. R. K.,* 'On the study of magneto-hydrodynamics boundary layer flow over a continuously moving flat plate', *Adv. Appl. Sci. Res,* ***4****(4), (2013), 279-282.*
4. *Jat R. N., Neemawat A., Rajotia D.,* 'MHD boundary layer flow and heat transfer over a continuously moving flat plate', *International Journal of Statistiika and Mathematika,* ***3****(3), (2012), 102-108.*
5. *Choi S.U.S.,* 'Enhancing thermal conductivity of fluids with nanoparticles –Developments and applications of non-Newtonian flows', *ASME, FED 231/MD,* ***66****, (1995), 99–105.*
6. *Eastman J.A., Choi S.U.S., Li S., Yu W.,* 'Anomalously increased effective thermal conductivity of ethylene glycol-based nanofluids containing copper nanoparticles', *Appl. Phys. Lett,* ***78****, (2001), 718 – 720.*
7. *Buongiorno J.,* 'Convective transport in nanofluids', *ASME J. Heat Trans,* ***128****, (2006), 240-250.*
8. *Mutuku-Njane W. N., Makinde O. D.,* 'On hydromagnetic boundary layer flow of nanofluids over a permeable moving surface with newtonian heating', *LAAR. in press, 2013.*
9. *Al-Sanea S.A.,* 'Mixed convection heat transfer along a continuously moving heated vertical plate with suction or injection', *Int. J. Heat Mass Transf,* ***47****, (2004), 1445–1465.*
10. *Poornima T., Reddy N. B.,* 'Radiation effects on MHD free convective boundary layer flow of nanofluids over a nonlinear stretching sheet', *Adv Appl Sci Res,* ***4****(2), (2013), 190-202.*
11. *Kandasamy R., Muhaimin I., Mohamad R.,* 'Thermophoresis and Brownian motion effects on MHD boundary-layerflow of a nanofluid in the presence of thermal stratification due to solar radiation', *Int J Mech Sci,* ***70****, (2013), 146–154.*
12. *Motsumi T.G., Makinde O.D.,* 'Effects of thermal radiation and viscous dissipation on boundary layer flow of nanofluids over a permeable moving flat plate', *Phys. Scr.* ***86*** *(2012).*
13. *Khan W.A., Pop I.,* 'Boundary-layer flow of a nanofluid past a stretching sheet', *Int. J. Heat Mass Transfer,* ***53****, (2010), 2477–2483.*
14. *Salleh M.Z., Nazar R., Pop I.,* 'Boundary Layer Flow and Heat Transfer over a Stretching Sheet with Newtonian Heating', *J Taiwan Inst. Chem. Eng.,* ***41****, (2010), 651−655.*